Available online at www.sciencedirect.com
SCIENCE DIRECT®
Acta Materialia 53 (2005) 4489–4496
Acta MATERIALIA
www.actamat-journals.com

Prediction of strong adhesion at the $MoSi_2$/Fe interface

D.E. Jiang [a], Emily A. Carter [a,b,*]

[a] Department of Chemistry and Biochemistry, Box 951569, University of California, Los Angeles, CA 90095-1569, USA
[b] Department of Mechanical and Aerospace Engineering and Program in Applied and Computational Mathematics, Princeton University, Princeton, NJ 08544-5263, USA

Received 10 May 2005; accepted 3 June 2005
Available online 11 August 2005

Abstract

We report a spin-polarized periodic density functional theory investigation of the atomic structure, bonding, and ideal work of adhesion of the $MoSi_2$/Fe interface, in order to explore the potential of $MoSi_2$ as a protective coating for steel. We find that $MoSi_2$ strongly adheres to Fe, with an ideal work of adhesion of $\sim$3.85 J/m^2 for two low-index, low-strain interfaces. This value will be a lower bound to measured adhesion energies, since the latter will be larger due to plasticity. This ideal adhesion energy for a ceramic coating to Fe is much stronger than predicted previously for ceramic coating materials such as ZrC and TiC. We attribute this stronger adhesion to increased covalent interfacial bonding for $MoSi_2$/Fe compared to metal carbide/Fe interfaces (where metallic bonding plays a larger role), as evidenced by the rearrangement of electron density and the character of the local density of states upon formation of the interface.

Keywords: Interfacial adhesion; Iron; Molybdenum disilicide; First principles electronic structure

1. Introduction

Structural units mainly made of steel often have to operate in harsh environments, at high temperatures and pressures, and in the presence of corrosive gases or liquids. Those units include pressure vessels and tubing, gas and oil pipelines, and gun barrels. The alloying of steel can improve its corrosion resistance under ambient conditions, but a protective coating is needed to protect ferritic steels from high temperature attack. For example, the use of stainless steel is not enough to withstand high temperatures and corrosive propellant gases present inside gun barrels. Instead, an electroplated Cr coating (melting point 1857 °C) is used to protect gun tubes (which are made of low alloy steels, melting point $\sim$1500 °C). Unfortunately, the electroplating process produces Cr coatings that have microcracks. These microcracks grow and propagate to the substrate metal during operation, allowing deleterious gases to travel along those cracks, subsequently attacking the substrate [1]. Another disadvantage of Cr coatings is their toxicity, due to production of Cr(VI)-containing ions or compounds.

Thus, alternative coatings are needed to protect steels from high temperature operating conditions. Desirable features of good coatings include strong adhesion to the substrate, similar coefficients of thermal expansion to that of the substrate, and resistance to fracture after thermal and mechanical cycling or shocks. Previous work from our group explored several types of ceramic coatings, including carbides (ZrC [2] and TiC [3]) and nitrides (BN). Here, we consider another type of refractory material, namely metal silicides, focusing on $MoSi_2$ in particular.

Due to its high melting point (2030 °C), high-temperature oxidation resistance, and its brittle-to-ductile

* Corresponding author. Tel.: +1 609 258 5391; fax: +1 609 258 5877.
E-mail address: eac@princeton.edu (E.A. Carter).

1359-6454/$30.00
doi:10.1016/j.actamat.2005.06.001

transition, $MoSi_2$ offers the potential as both a high-temperature structural material [4] and a high-temperature coating for industrial and military applications [5]. Although $MoSi_2$ was first discovered in 1907 [6] when it was tested for use as a high-temperature protective coating for ductile metals against corrosion, improvement of $MoSi_2$ as a coating is still actively pursued today [7].

A great deal of work [2,3,8–39] on ceramic/metal interfaces has been carried out using first principles methods, primarily density functional theory (DFT). Most investigations of ceramics have considered oxides (e.g., MgO, Al_2O_3, SiO_2, and ZrO_2) [8–14,17–25,27–29,31–38], carbides (e.g., TiC, ZrC, and WC) [2,3,12,15,16,26,28,30,39], and nitrides (e.g., TiN and CrN) [12,28,39] rather than silicides. The electronic structure and bonding of bulk $MoSi_2$ has been subject of many DFT studies [40–46]. In agreement with experiment, $MoSi_2$ was found to have a pseudo-gap and a low but nonzero density of states at the Fermi level. Good agreement with experiment for lattice parameters, elastic constants, and cohesive energy also was achieved.

In this work, we examine the structure, bonding, and energetics of the $MoSi_2$/Fe interface with first principles DFT techniques. The rest of the paper is laid out as follows. We give calculational details in Section 2, followed by results and discussion in Section 3, and we summarize in Section 4.

2. Calculational details

We performed DFT calculations [47,48] within both the local density approximation (LDA) and the generalized gradient approximation (GGA) due to Perdew, Burke, and Ernzerhof (PBE) [49] for electron exchange and correlation, using the Vienna ab initio simulation package [50,51]. We employed Blöchl's all-electron projector augmented wave (PAW) method [52], as implemented by Kresse and Joubert [53]. We used the standard version of the PAW potentials for Fe, Mo, and Si supplied with VASP for both the LDA and the PBE form of the GGA [49].

We tested k-point sampling and kinetic energy cutoff convergence for bulk, surface, and interface supercells. As a result, we used a kinetic energy cutoff of 400 eV for all calculations, which converged total energies to within 1 meV/atom for bulk Fe and $MoSi_2$. Using a converged $15\times15\times15$ k-mesh, we obtained an equilibrium lattice constant ($a_0 = 2.83$ Å), bulk modulus ($B =$ 174 GPa), and local magnetic moment ($M = 2.20\ \mu_B$) for ferromagnetic bcc Fe. The results agree very well with previous PAW-GGA calculations and experiment ($a_0 = 2.86$ Å, $B = 168$ GPa, $M = 2.22\ \mu_B$) [54]. We used a converged $12\times12\times6$ k-mesh for the orthorhombic unit cell of $MoSi_2$ (discussed further in Section 3.1).

For modeling surfaces and interfaces, we used a 10 Å thick vacuum layer and five layers of Fe substrate atoms. In surface energy calculations, the slab is allowed to fully relax, and is converged with respect to slab thickness. In the interface calculations, the bottom three layers are kept fixed at their bulk positions to model a semi-infinite crystalline substrate. Including the middle layer in the relaxation changes the slab energy only by $\sim$0.01 J/m^2. We used k-meshes of $4\times4\times1$ and $2\times2\times1$ for surfaces and interfaces of Fe(1 0 0) and Fe(1 1 0), respectively, which converged the adhesion energy to $\sim$0.005 J/m^2. To study the primitive cells of $MoSi_2$ surfaces, we used converged k-meshes of $10\times10\times1$, $12\times12\times1$, and $6\times12\times1$ for (1 1 0), (0 0 1), and (1 0 0), respectively. These particular low-index surfaces were examined, since they are the most stable and therefore the most likely to form.

The first-order Methfessel–Paxton method [55] was used for the Fermi-surface smearing in order to obtain accurate forces, and a smearing width of 0.1 eV was chosen such that the error in the extrapolated energy at 0 K is less than 1 meV/atom. The force tolerance for structural relaxation was set to 0.025 eV/Å.

The ideal adhesion energy is defined as $E_{adh} = (E_1 + E_2 - E_{12})/A$, where E_1, E_2, and E_{12} are the total energy of the isolated substrate, the isolated coating, and the interface, respectively, and A is the area. Here, we assume that the coating adapts to the lateral lattice vectors of the substrate both in the interface and as a separate slab. With this definition, we determine the ideal work of separation (neglecting plastic work and diffusion), where a positive E_{adh} implies an attractive interaction between the substrate and the coating. Due to limitations in the size of the simulation cell caused by the high cost of first principles calculations, small supercells with a large lattice misfit between the coating and the substrate are often used [16,28,38]. In these cases, the coating material is under strain, which may change its electronic structure and cause errors in the calculated ideal work of separation. We attempt to minimize the effects of such situations, as we now explain.

To study the $MoSi_2$/Fe interface, we have to choose appropriate surfaces of $MoSi_2$ and Fe to interact. We base our choice on two criteria. First, we consider only low-energy surfaces of $MoSi_2$ and Fe. Second, we limit the extent of lattice mismatch [21] to be less than 5%. The (1 1 0) and (0 0 1) surfaces are the two lowest-energy surfaces of $MoSi_2$ (see Section 3.1), while Fe(1 1 0) and Fe(1 0 0) are the two Fe surfaces with lowest energy [3]. We find that the best match (least mismatch strain) is between Fe(1 0 0) and $MoSi_2$(0 0 1) (lattice mismatch $\sim$1.5% for an area of 40 Å^2, where $MoSi_2$ is under a small compressive strain); we examine this interface in Section 3.2. The next best is between Fe(1 1 0) and $MoSi_2$(1 1 0) (lattice mismatch $\sim$1.7% for an area of 91 Å^2, with $MoSi_2$ under a small tensile

strain). Because Fe(1 1 0) and $MoSi_2$(1 1 0) are the lowest-energy surfaces of Fe and $MoSi_2$, we also investigate this interface (Section 3.3). With ~1.5–1.7% lattice misfit due to finite size, we estimate the error in the calculated adhesion energy is ~5%, based on a simple dimensional analysis (energy ∝ volume^2 ∝ area^3; lattice misfit representing an error in area).

3. Results and discussion

3.1. Bulk and surface properties of $MoSi_2$

$MoSi_2$ has a body-centered tetragonal structure (C11b), as shown in Fig. 1, where one Mo layer is sandwiched by two Si layers. To benchmark our level of theory, we display our results for the structural properties of $MoSi_2$ in Table 1. We see that DFT-PAW-GGA-PBE gives lattice parameters and a bulk modulus that compare well with experiment. DFT-PAW-LDA also yields reasonable results, exhibiting the usual LDA overbinding that produces lattice parameters that are too short and a bulk modulus that is too large. Because GGA is necessary to accurately describe the bulk properties of ferromagnetic body-centered-cubic Fe [54], we use the PBE form of GGA for all of the following work.

We consider several low Miller-index surfaces of $MoSi_2$, including (1 1 0), (1 0 0), and (0 0 1) (Fig. 2).

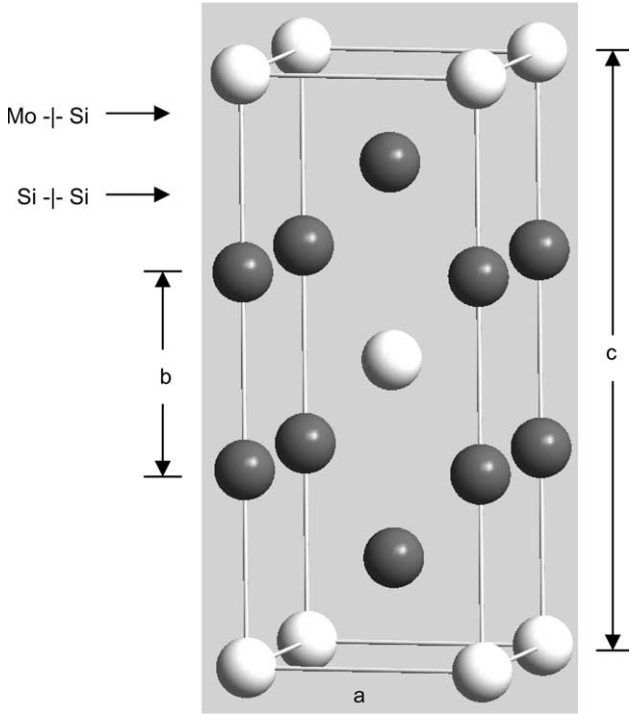

Fig. 1. Bulk structure of $MoSi_2$. Si atoms in dark grey and Mo in white.

Table 1
Bulk properties of $MoSi_2$: lattice parameters for the tetragonal cell (a, b, and c) and bulk modulus (B)

Method	a (Å)	b (Å)	c (Å)	B (GPa)
PAW-LDA	3.175	2.562	7.778	229
PAW-GGA-PBE	3.215	2.592	7.865	207
Experiment[a]	3.198	2.618	7.859	210

See Fig. 1 for the definitions of a, b, and c.

[a] Room temperature data for lattice parameters [56] are extrapolated to zero K by using the measured coefficient of thermal expansion of $MoSi_2$ of 7×10^{-6}/K [57].

First, we examine $MoSi_2$(0 0 1). There are two ways to cleave a pair of atomic planes to generate $MoSi_2$(0 0 1), as shown in Fig. 1 (Mo-|-Si and Si-|-Si). The former cleavage results in a surface slab terminated with Si on one side and Mo on the other side, while the latter leads to a surface terminated with Si on both sides (Fig. 2(b)). Table 2 displays the fracture energies, defined as the sum of the energies of the two newly exposed surfaces, for a six-layer slab. Not surprisingly, they differ for those two cleavage planes. We find that it is much easier to cleave the Si–Si pair of planes, for both bulk-terminated (unrelaxed) and relaxed surfaces. In other words, the bonding between Mo and Si is much stronger than between Si and Si in $MoSi_2$. This finding agrees with the study of bulk $MoSi_2$ bonding by Bhattacharyya et al. [40], Andersen et al. [44], and Alouani et al. [46] using DFT-LDA. By analyzing charge density plots, they inferred that Si–Si bonds are weaker than Mo–Si bonds in bulk $MoSi_2$. So we would expect that $MoSi_2$(0 0 1) preferentially exposes a single Si layer. This is exactly what high-resolution core-level and valence-band photoemission experiments have shown [58]. Moreover, no reconstruction has been observed in this Si layer, as determined by low-energy electron diffraction (LEED) [59].

Both $MoSi_2$(1 1 0) and $MoSi_2$(1 0 0) have unique structures, each with only one possible cleavage plane, and their structures are shown in Fig. 2 with that of $MoSi_2$(0 0 1). We see that both surfaces are stoichiometric, in contrast to the (0 0 1) Si-terminated surface. LEED patterns indicate that $MoSi_2$(1 1 0) is bulk-terminated, implying no reconstruction at this surface [60]. Unfortunately, we have found no measurements reported for single crystal $MoSi_2$(1 0 0), so we have assumed that this surface does not reconstruct, like its other low-index counterparts. Table 3 displays the surface energies for those three surfaces. $MoSi_2$(1 1 0) has the lowest surface energy, followed by (0 0 1), and then (1 0 0). This is consistent with the fact that $MoSi_2$(1 1 0) has a much higher packing density than $MoSi_2$(0 0 1) or $MoSi_2$(1 0 0). Even though the packing density of $MoSi_2$(1 0 0) (see Table 3) is higher than that of $MoSi_2$(0 0 1), the latter has a lower surface energy. This is likely due to the fact that $MoSi_2$(0 0 1)

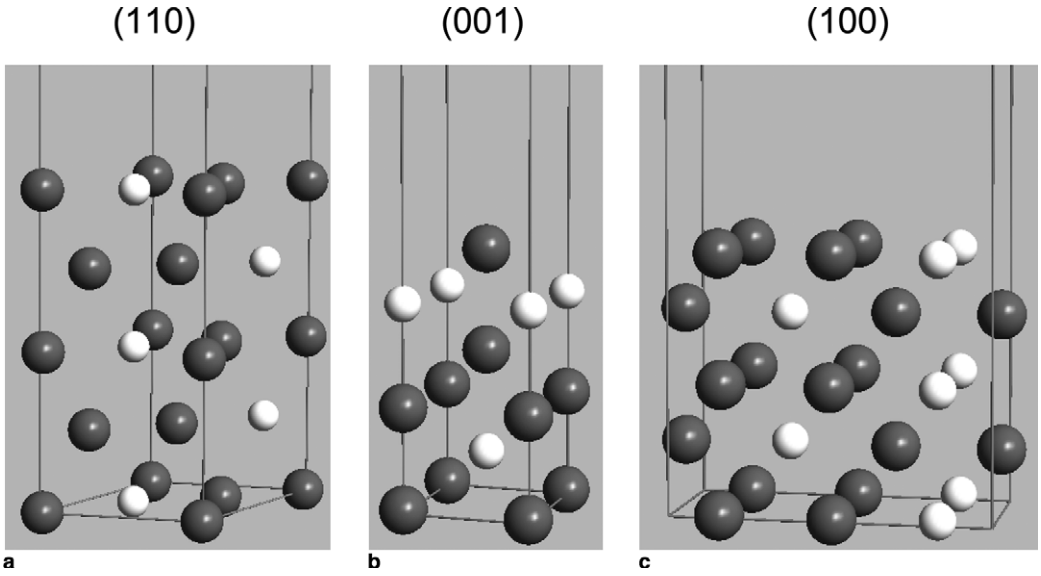

Fig. 2. Surface structures of $MoSi_2$. Si atoms in dark grey and Mo in white.

Table 2
Fracture energy (E_{frct}) of $MoSi_2$(0 0 1) between two different pairs of atomic planes

Fracture plane pair	Mo-|-Si	Si-|-Si
Unrelaxed E_{frct} (J/m^2)	7.266	4.733
Relaxed E_{frct} (J/m^2)	7.053	4.639

Table 3
Surface energies (γ) and packing density (θ) of several low Miller-index surfaces of $MoSi_2$

Properties	(1 1 0)	(0 0 1)	(1 0 0)
γ (J/m^2): unrelaxed	2.261	2.367	2.779
γ (J/m^2): relaxed	2.185	2.320	2.657
θ (atoms/Å^2)	0.168	0.097	0.119

is Si-terminated and Si–Si bonds are weaker than Mo–Si bonds, as discussed above.

3.2. Adhesion of $MoSi_2$(0 0 1)/Fe(1 0 0)

We know from Section 3.1 that $MoSi_2$ prefers to cleave between two neighboring Si planes in the [0 0 1] direction. Therefore, $MoSi_2$(0 0 1) is Si-terminated, followed by Mo in the nearest subsurface layer, and then a Si layer again appears. When we adhere $MoSi_2$(0 0 1) to Fe(1 0 0), we use multiples of this Si–Mo–Si sandwich structure, namely Si-terminated layers at both the interface and the free surface, and allow all the atoms in the coating to relax subject to the substrate surface lattice vector constraints. Fig. 3(a) displays how the adhesion energy changes with the number of layers in the $MoSi_2$ slab. We see that the adhesion energy reaches its asymptotic value of 3.84 J/m^2 at six layers of $MoSi_2$ (or two multiples of the Si–Mo–Si sandwich structure). From six layers to nine layers, the adhesion energy is basically unchanged, indicating the interfacial bonding is fairly local. This adhesion energy of 3.84 J/m^2 is quite strong; we will compare this value with those from other ceramic coatings in the next section.

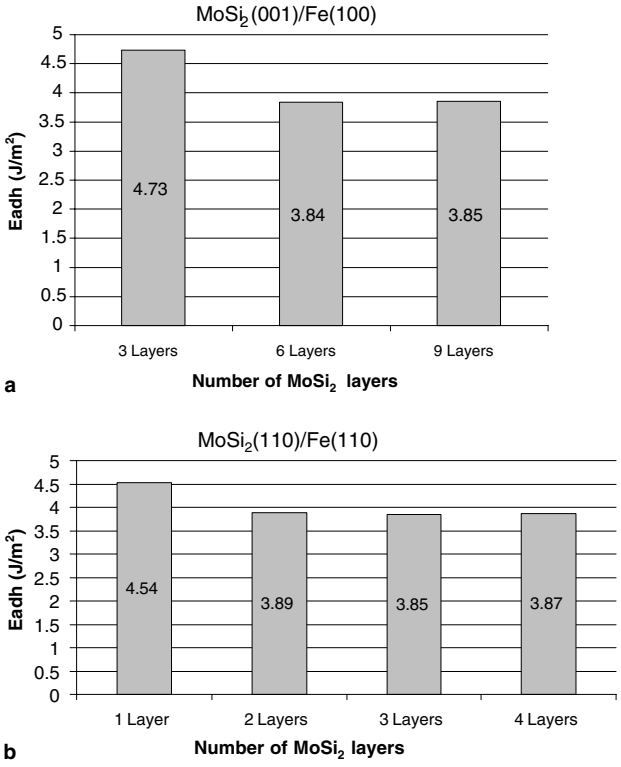

Fig. 3. Convergence of adhesion energy vs. layer thickness: (a) $MoSi_2$(0 0 1)/Fe(1 0 0); (b) $MoSi_2$(1 1 0)/Fe(1 1 0).

Fig. 4 shows the structural relaxation of $MoSi_2$(0 0 1)/Fe(1 0 0). One striking feature is that all the Si atoms at the interface adapt to the surface structure of the Fe substrate and move to occupy the fourfold hollow sites. After Si occupies those sites, one hollow site is still open for each unit cell and one Mo atom in the second coating layer near the interfacial layer of Si atoms moves toward the open hollow site at the interface (Fig. 4(d) and (e)).

When matching two surfaces to obtain an interface, the relative lateral positions of the atoms are adjustable. We tried several different relative lateral positions; they all ended up with the same final structure. This is likely due to the strong site selectivity at the $MoSi_2$(0 0 1)/Fe(1 0 0) interface: the interfacial Si atoms strongly prefer the hollow sites of the Fe substrate. This strong site selectivity is suggestive of localized covalent bonding between the Si atoms and the Fe surface, as we now demonstrate.

Fig. 5(a) displays an electron density difference plot for the interface. We see that the rearrangement of electron density takes place primarily at the interface, indicating again that the interfacial bonding is local. Electron density is depleted from the interfacial Fe atoms, while accumulating at the interface between Fe and Si. The accumulated electron density is localized between Fe and Si atoms, reminiscent of covalent bonding. The local density of states (LDOS) for Fe

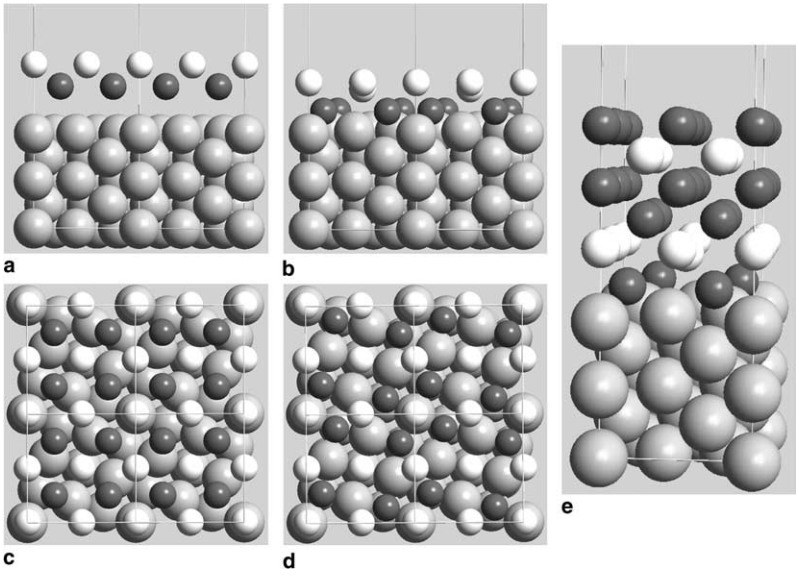

Fig. 4. Relaxation of the $MoSi_2$(0 0 1)/Fe(1 0 0) interface: (a) side view of the initial structure; (b) side view of the final structure; (c) top view of the initial structure; (d) top view of the final structure; (e) side view of the complete final structure. In (a), (b), (c), and (d), only the two $MoSi_2$(0 0 1) layers at the interface are shown, and the other four layers of $MoSi_2$(0 0 1) are hidden, for ease of viewing. Fe atoms are in light grey, Si in dark grey, and Mo in white. The same color scheme for atoms is used in all subsequent figures.

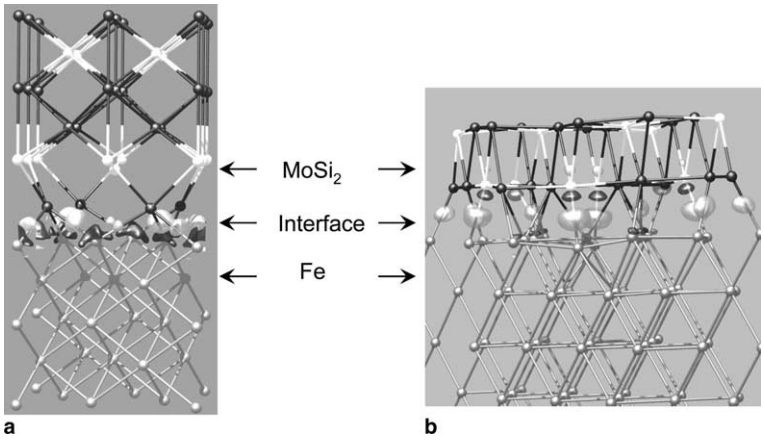

Fig. 5. Isosurface plot of the electron density difference, $\Delta\rho$, for (a) $MoSi_2$(0 0 1)/Fe(1 0 0) and (b) $MoSi_2$(1 1 0)/Fe(1 1 0). The isosurface values are at ± 0.075 e/Å^3 for (a) and ± 0.10 e/Å^3 for (b). The light grey surface has the positive value, and the dark grey surface has the negative value. Negative $\Delta\rho$ indicates loss of electron density upon adhesion. Solid balls represent atoms.

and Si atoms at the interface is displayed in Figs. 6(a) and (b). We see that Si 3s states are found primarily below −6.5 eV, whereas Si 3p states strongly overlap both the occupied (bonding) Fe 4sp states (Fig. 6(a)) and the occupied (bonding) Fe 3d states (Fig. 6(b)) above −6.5 eV, with a concomitant overlap of unoccupied (antibonding) Fe 4sp and 3d and Si 3s and 3p states at +1 to +3 eV, a clear signature of covalent bonding. The LDOS of Fe at the interface shows significant amplitude at the Fermi level, similar to that of bulk Fe (not shown), indicating that metallic Fe–Fe bonding is retained at the interface, despite some depletion of electron density shown in Fig. 5(a). It is likely that the covalent character of Fe–Si interfacial bonding accounts for the strong adhesion at $MoSi_2$(0 0 1)/Fe(1 0 0). Consistent with our findings, Smith et al. also noted covalent character between metal and Si atoms across a Mo/$MoSi_2$ interface when studying effects of impurities at the interface with DFT-LDA [61].

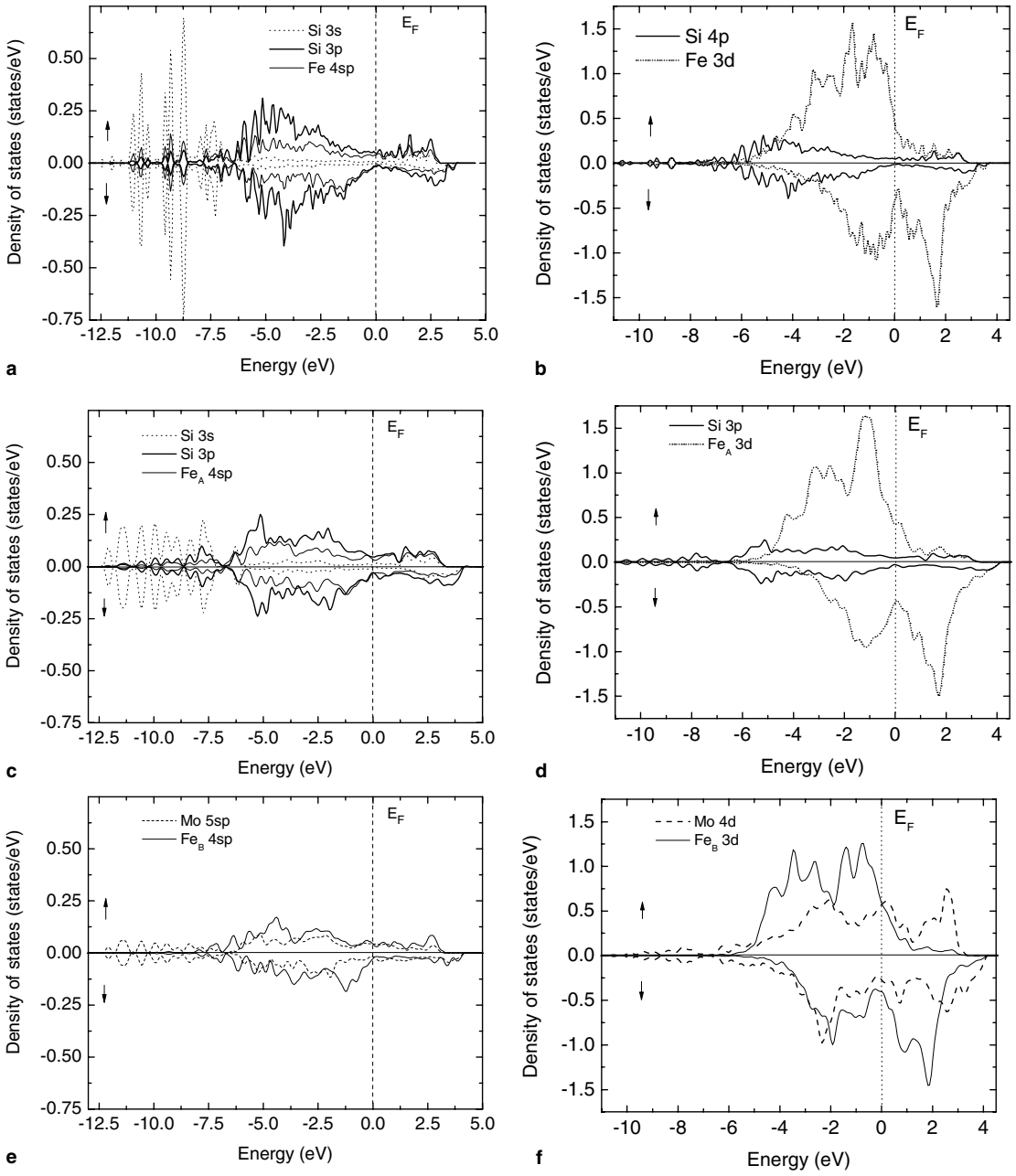

Fig. 6. Spin-polarized local density of states (LDOS) for: a Si atom and a nearest neighbor Fe atom at the $MoSi_2$(0 0 1)/Fe(1 0 0) interface [(a) and (b)]; a Si atom and a nearest neighbor Fe atom (Fe_A) at the $MoSi_2$(1 1 0)/Fe(1 1 0) interface [(c) and (d)]; a Mo atom and a nearest neighbor Fe atom (Fe_B) at the $MoSi_2$(1 1 0)/Fe(1 1 0) interface [(e) and (f)].

3.3. Adhesion of $MoSi_2$(1 1 0)/Fe(1 1 0)

$MoSi_2$(1 1 0) is the closest-packed surface of $MoSi_2$. Each layer of $MoSi_2$(1 1 0) has a 1:2 stoichiometry of Mo and Si atoms, respectively. As a result, fewer layers turn out to be needed to reach an asymptotic value of the ideal adhesion energy (Fig. 3(b)). We see that a thin film of three layers of $MoSi_2$(1 1 0) has an ideal adhesion energy of 3.85 J/m^2, very similar to that of $MoSi_2$(0 0 1)/Fe(1 0 0). Our group has studied other refractory coatings on Fe, such as ZrC and TiC. We find that $MoSi_2$ adheres much more strongly to Fe than does ZrC (2.30 J/m^2) [2] or TiC (2.56 J/m^2) [3].

Structural relaxation of $MoSi_2$(1 1 0)/Fe(1 1 0) is less dramatic than for $MoSi_2$(0 0 1)/Fe(1 0 0), due to two reasons. First, $MoSi_2$(1 1 0) and Fe(1 1 0) are the closest-packed surfaces of $MoSi_2$ and Fe. Second, the $MoSi_2$(1 1 0)/Fe(1 1 0) interface is more metallic in nature (as the LDOS shows below). The more delocalized electron density results in less structural relaxation and weaker site selectivity. We find that the final structure of $MoSi_2$(1 1 0)/Fe(1 1 0) depends on the initial relative lateral matching position. Unlike $MoSi_2$(1 0 0)/Fe(1 0 0), where strong site selectivity leads to the same final structure, $MoSi_2$(1 1 0)/Fe(1 1 0) tends to relax to the local minimum closest to the initial structure. Nevertheless, three different initial structures (Fig. 7) yield a variation of only ~0.07 J/m^2 in the ideal adhesion energy.

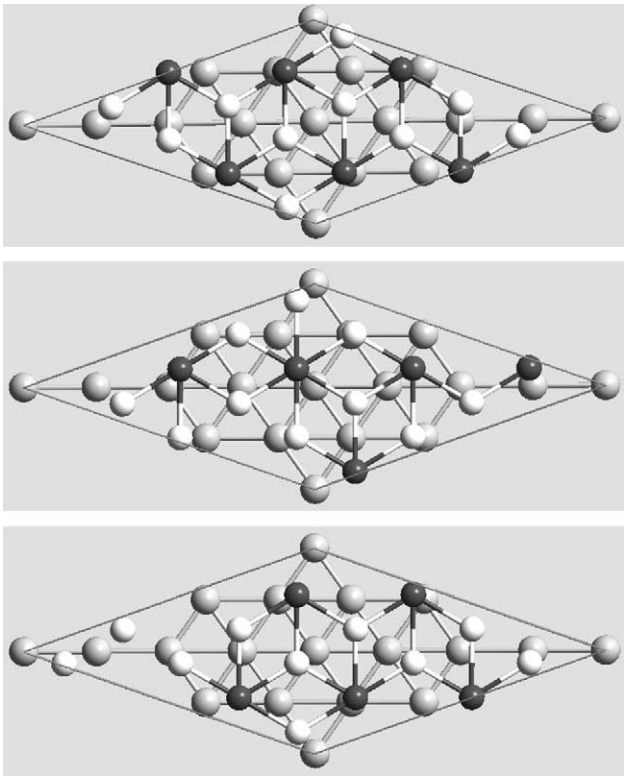

Fig. 7. Three distinct initial structures for relaxation of the $MoSi_2$(1 1 0)/Fe(1 1 0) interface. The resultant ideal adhesion energies are 3.85, 3.78, and 3.81 J/m^2 for the top, middle, and bottom configurations, respectively.

Fig. 5(b) displays an electron density difference plot for the interface. Again, the rearrangement of electron density happens primarily at the interface. Electron density is depleted from interfacial Fe and Mo atoms, while accumulating at the interface in Fe–Si and Fe–Mo bonds. Here, we see the localized, covalent character of interfacial bonding again. The importance of covalent bonding for strong metal–ceramic interfaces has been noted earlier [2,3,24,25,27].

We also analyzed the LDOS at the $MoSi_2$(1 1 0)/Fe(1 1 0) interface (Figs. 6(c)–(f)). The hybridization of Fe 4sp states with Si 3sp states (Fig. 6(c)) and Fe 3d states with Si 3p states (Fig. 6(d)) at the interface is similar to that of $MoSi_2$(0 0 1)/Fe(1 0 0), but the extent of mixing is less, with Si 3sp states more dispersed at this (1 1 0)/(1 1 0) interface. However, the mixing between Fe 4sp and Mo 5sp states (Fig. 6(e)) and Fe 3d and Mo 4d states (Fig. 6(f)) is strong below and near the Fermi level, respectively, indicating that metallic bonding across the interface between Fe and Mo plays a significant role. Thus, lowered covalent bonding between Fe and Si at the $MoSi_2$(1 1 0)/Fe(1 1 0) interface is compensated for by metallic bonding between Fe and Mo, yielding an adhesion energy similar to $MoSi_2$(0 0 1)/Fe(1 0 0).

4. Summary

Since $MoSi_2$ has potential as a high-temperature coating for steel, we examined the structure, bonding, and energetics associated with the $MoSi_2$/Fe interface using periodic DFT. We found that bulk $MoSi_2$ is well described with DFT-GGA and determined that $MoSi_2$(0 0 1) is preferentially Si-terminated. We predict that the lowest-energy low-index surface of $MoSi_2$ is the closest-packed (1 1 0), followed by (0 0 1), and then (1 0 0). We predict $MoSi_2$ adheres strongly to Fe with adhesion energy of ~3.85 J/m^2 for both $MoSi_2$(0 0 1)/Fe(1 0 0) and $MoSi_2$(1 1 0)/Fe(1 1 0) interfaces. Changes in the electron density upon formation of the interface are highly localized between Fe–Si and Fe–Mo. The mixing of Fe sp and d-states with Si p-states at the interface suggests covalent bonding at the interface, while the hybridization between Fe and Mo d-states shows metallic character across the interface. It is this mixed bonding that accounts for the strong adhesion between $MoSi_2$ and Fe. $MoSi_2$(1 1 0)/Fe(1 1 0) shows weak site selectivity of the substrate surface partly due to the more metallic nature of the interfacial bonding, whereas $MoSi_2$(0 0 1)/Fe(1 0 0) shows strong site selectivity because of significant covalent character at the interface.

From the standpoint of strong interfacial bonding, our work indicates that $MoSi_2$ is a promising alternative to chrome as a high-temperature coating for steel. This conclusion may be true also for other metal silicides such as WSi_2. Even though metal silicides tend to be brittle at low temperatures, the brittle-to-ductile transition temperature can be lowered by alloying with other elements [62–65]. Moreover, $MoSi_2$-based composite materials have been explored to improve the mechanical properties of $MoSi_2$ [4]. Although some technical difficulties remain to be overcome, the intrinsic strength of the $MoSi_2$/Fe interface determined here is an encouraging indicator for future use of $MoSi_2$ as a high-temperature protective coating.

Acknowledgements

This work was supported by the Army Research Office. We thank the Maui High Performance Computing Center and the ARL Major Shared Resources Center for providing CPU time.

References

[1] Cote PJ, Rickard C. Wear 2000;241:17.
[2] Arya A, Carter EA. Surf Sci 2004;560:103.
[3] Arya A, Carter EA. J Chem Phys 2003;118:8982.
[4] Petrovic JJ, Vasudevan AK. Mater Sci Eng 1999;A261:1.
[5] Kircher TA, Courtright EL. Mater Sci Eng A 1992;155:67.
[6] Hoenigsschmid O. Monatsh Chem 1907;28:1017.
[7] Yoon JK, Lee KH, Kim GH, Lee JK, Doh JM, Hong KT. J Electrochem Soc 2004;151:B309.
[8] Hong T, Smith JR, Srolovitz DJ. Acta Metall Mater 1995;43:2721.
[9] Finnis MW. J Phys Condens Matter 1996;8:5811.
[10] Pacchioni G, Rosch N. J Chem Phys 1996;104:7329.
[11] Ikuhara Y, Sugawara Y, Tanaka I, Pirouz P. Interf Sci 1997;5:5.
[12] Mizuno M, Tanaka I, Adachi H. Acta Mater 1998;46:1637.
[13] Benedek R, Seidman DN, Minkoff M, Yang LH, Alavi A. Phys Rev B 1999;60:16094.
[14] Purton JA, Bird DM, Parker SC, Bullett DW. J Chem Phys 1999;110:8090.
[15] Kohyama M, Hoekstra J. Mater Sci Forum 1999;294(2):95.
[16] Dudiy SV, Hartford J, Lundqvist BI. Phys Rev Lett 2000;85:1898.
[17] Batyrev IG, Alavi A, Finnis MW. Phys Rev B 2000;62:4698.
[18] Benedek R, Alavi A, Seidman DN, Yang LH, Muller DA, Woodward C. Phys Rev Lett 2000;84:3362.
[19] Smith JR, Zhang W. Acta Mater 2000;48:4395.
[20] Jarvis EAA, Christensen A, Carter EA. Surf Sci 2001;487:55.
[21] Christensen A, Carter EA. J Chem Phys 2001;114:5816.
[22] Ochs T, Kostlmeier S, Elsasser C. Integr Ferroelectr 2001;32:959.
[23] Zhang W, Smith JR, Evans AG. Acta Mater 2002;50:3803.
[24] Jarvis EA, Carter EA. Phys Rev B 2002;66:100103.
[25] Jarvis EAA, Carter EA. J Phys Chem B 2002;106:7995.
[26] Christensen M, Dudiy S, Wahnstrom G. Phys Rev B 2002; 65:045408.
[27] Jarvis EAA, Carter EA. J Am Ceram Soc 2003;86:373.
[28] Siegel DJ, Hector LG, Adams JB. Phys Rev B 2003;67:092105.
[29] Lopez N, Valeri S. Phys Rev B 2004;70:125428.
[30] Liu LM, Wang SQ, Ye HQ. J Phys Condens Matter 2004;16:5781.
[31] Tanaka S, Yang R, Kohyama M, Sasaki T, Matsunaga K, Ikuhara Y. Mater Trans 2004;45:1973.
[32] Finnis MW, Kruse C, Schonberger U. Nanostruct Mater 1995;6:145.
[33] Zhao GL, Smith JR, Raynolds J, Srolovitz DJ. Interf Sci 1996;3:289.
[34] Schweinfest R, Kostlmeier S, Ernst F, Elsasser C, Wagner T, Finnis MW. Philos Mag A 2001;81:927.
[35] Siegel DJ, Hector LG, Adams JB. Phys Rev B 2002;65:085415.
[36] Kostlmeier S, Elsasser C, Meyer B, Finnis MW. Phys Status Solidi A – Appl Res 1998;166:417.
[37] Zhang W, Smith JR. Phys Rev B 2000;61:16883.
[38] Ricci D, Pacchioni G. Phys Rev B 2004;69:161307.
[39] Dudiy SV, Lundqvist BI. Phys Rev B 2001;64:045403.
[40] Bhattacharyya BK, Bylander DM, Kleinman L. Phys Rev B 1985;32:7973.
[41] Li BQ, Ji MR, Wu JX, Hsu CC, Yian J. Chinese Phys 1990;10:481.
[42] Mattheiss LF. Phys Rev B 1991;43:12549.
[43] McMahan AK, Klepeis JE, Vanschilfgaarde M, Methfessel M. Phys Rev B 1994;50:10742.
[44] Andersen OK, Jepsen O, Antonov VN, Yavorsky BY, Perlov AY, Shpak AP. Physica B 1995;204:65.
[45] Imai Y, Mukaida M, Tsunoda T. Intermetallics 2000;8:381.
[46] Alouani M, Albers RC, Methfessel M. Phys Rev B 1991;43:6500.
[47] Hohenberg P, Kohn W. Phys Rev 1964;136:B864.
[48] Kohn W, Sham LJ. Phys Rev 1965;140:A1133.
[49] Perdew JP, Burke K, Ernzerhof M. Phys Rev Lett 1996;77:3865.
[50] Kresse G, Furthmüller J. Phys Rev B 1996;54:11169.
[51] Kresse G, Furthmüller J. Computat Mater Sci 1996;6:15.
[52] Blöchl PE. Phys Rev B 1994;50:17953.
[53] Kresse G, Joubert D. Phys Rev B 1999;59:1758.
[54] Jiang DE, Carter EA. Phys Rev B 2003;67:214103.
[55] Methfessel M, Paxton AT. Phys Rev B 1989;40:3616.
[56] Villars P, Calvert LD. Pearson's handbook of crystallographic data for intermetallic phases. Metals Park (OH): American Society for Metals; 1985.
[57] Conzone SD, Butt DP, Bartlett AH. J Mater Sci 1997;32:3369.
[58] Komeda T, Hirano T, Waddill GD, Anderson SG, Sullivan JP, Weaver JH. Phys Rev B 1990;41:8345.
[59] Sullivan JP, Hirano T, Komeda T, Meyer HM, Trafas BM, Waddill GD, et al. Appl Phys Lett 1990;56:671.
[60] Johansson HIP, Hakansson KL, Johansson LI, Christensen AN. Phys Rev B 1994;49:7484.
[61] Hong T, Smith JR, Srolovitz DJ. Phys Rev B 1993;47:13615.
[62] Waghmare UV, Kaxiras E, Bulatov VV, Duesbery MS. Model Simul Mater Sci Eng 1998;6:493.
[63] Arvanitis A, Diplas S, Tsakiropoulos P, Watts JF, Whiting MJ, Morton SA, et al. Acta Mater 2001;49:1063.
[64] Sharif AA, Misra A, Petrovic JJ, Mitchell TE. Intermetallics 2001;9:869.
[65] Woolman JN, Petrovic JJ, Munir ZA. Scripta Mater 2003; 48:819.